JACS Au
AN OPEN ACCESS JOURNAL OF THE AMERICAN CHEMICAL SOCIETY

pubs.acs.org/jacsau

Article

Bifurcated Halogen Bonding Involving Two Rhodium(I) Centers as an Integrated σ-Hole Acceptor

Anastasiya A. Eliseeva, Daniil M. Ivanov, Anton V. Rozhkov, Ivan V. Ananyev, Antonio Frontera,* and Vadim Yu. Kukushkin*

Cite This: *JACS Au* 2021, 1, 354–361

Read Online

ACCESS | Metrics & More | Article Recommendations | Supporting Information

ABSTRACT: The complexes $[RhX(COD)]_2$ (X = Cl, Br; COD = 1,5-cyclooctadiene) form cocrystals with σ-hole iodine donors. X-ray diffraction studies and extensive theoretical considerations indicate that the d_z^2-orbitals of two positively charged rhodium(I) centers provide sufficient nucleophilicity to form a three-center halogen bond (XB) with the σ-hole donors. The two metal centers function as an integrated XB acceptor, providing assembly via a metal-involving XB.

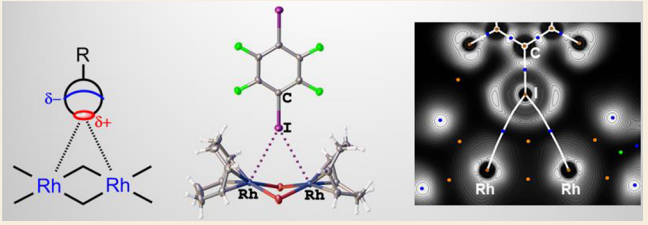

KEYWORDS: *noncovalent interactions, metal-involving halogen bonding, rhodium cocrystals, bifurcate, assembly*

INTRODUCTION

Halogen bonding (XB)[1,2]—together with other types of noncovalent interactions (see a special issue of *Chemical Reviews* 2016, Issue 9, and also reviews[3−7])—has exponentially emerged as an important concept in supramolecular design and crystal engineering,[8−10] synthetic coordination chemistry,[11] polymer science,[12] XB-involving catalysis,[13−16] medicinal chemistry,[17,18] and human physiology.[19]

According to the IUPAC definition,[1] XB is a net attractive interaction between an electrophilic region (σ-hole; abbreviated as σh) associated with a halogen atom (XB donor) and a nucleophilic region on an XB-accepting center. Organic iodine(I)-based species, R^{EWG}–I, featuring electron-withdrawing groups (EWG) are the most often employed as σh donors, while commonly applied XB acceptors predominantly include electronegative heteroatoms bearing lone pair(s) and electron-donating carbon-based π-systems. Much less common is the application of positively charged d_z^2-orbital-donating metal centers as XB acceptors.

To date, metal-involving two-center XBs have been recognized for Ni^{II},[20,21] Pd^{II},[21−23] Pt^{II},[23−28] Au^0,[29,30] and Au^I.[31] In a few instances, a M^{II} center and the adjacent coordinated nonmetal atom function as an integrated XB acceptor to give three-center bifurcated μ_2-X···[Pt^{II},Cl] (X = Br, I)[25,26] and μ_2-I···[Pt^{II},C][28] linkages.

If XBs of iodine(I)-based σh donors with d^8-metals such as Pd^{II} and Pt^{II} are not unusual although still uncommon, similar contacts with rhodium(I) centers are nearly unique—the only one identified short contact between a Rh^I center and an iodine atom of I_2[32,33] belongs to the category of coordinative,[34] rather than conventional, XB.[1]

We now report that simultaneous action of the d_z^2-orbitals of two positively charged rhodium(I) centers provides sufficient nucleophilicity to form three-center XB with the σh-donating iodine(I)-based organic species. This is the first example of three-center XB, where two metal centers function as an integrated XB acceptor, providing assembly via XBs.

RESULTS AND DISCUSSION

The $[RhX(COD)]_2$ (X = Cl, Br; COD = 1,5-cyclooctadiene) complexes were cocrystallized with various iodine(I)-based σh donors, namely, 1,4-diiodotetrafluorobenzene ($C_6F_4I_2$), nonafluoro-4-iodo-1,1′-biphenyl ($C_{12}F_9I$), tetraiodoethylene (C_2I_4), and iodoform (CHI_3), to give the cocrystals[35] $[RhCl(COD)]_2\cdot(C_6F_4I_2)$ (**1**), $[RhBr(COD)]_2\cdot 0.5(C_6F_4I_2)$ (**2**), $[RhCl(COD)]_2\cdot(C_{12}F_9I)$ (**3**), $[RhCl(COD)]_2\cdot 1.5(C_2I_4)$ (**4**), and $[RhCl(COD)]_2\cdot(CHI_3)$ (**5**) studied by single-crystal X-ray diffraction (XRD; Section S1, Supporting Information).

In the structure of **1**, two iodine centers from two $C_6F_4I_2$ are linked to the Rh_2Cl_2 core of the complex (Figure 1a), whereas in **2**–**5**, Rh_2X_2 (X = Cl, Br) entities interact with only one I of an appropriate σh donor (Figure 1b–e). In the case of **1**, when the interaction with the iodine atoms occurs above and below the Rh_2Cl_2 plane, the metal core is perfectly planar (r.m.s. deviation 0.000 Å). In **2**–**5**, the Rh_2X_2 functionality deviates from the planarity, with the Rh atoms tilted toward iodine centers of R^{EWG}–I species; the largest r.m.s. deviation of the core was found in **5** (0.302 Å for Br1).

Received: January 11, 2021
Published: February 19, 2021

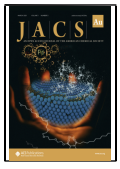

https://dx.doi.org/10.1021/jacsau.1c00012
JACS Au 2021, 1, 354–361

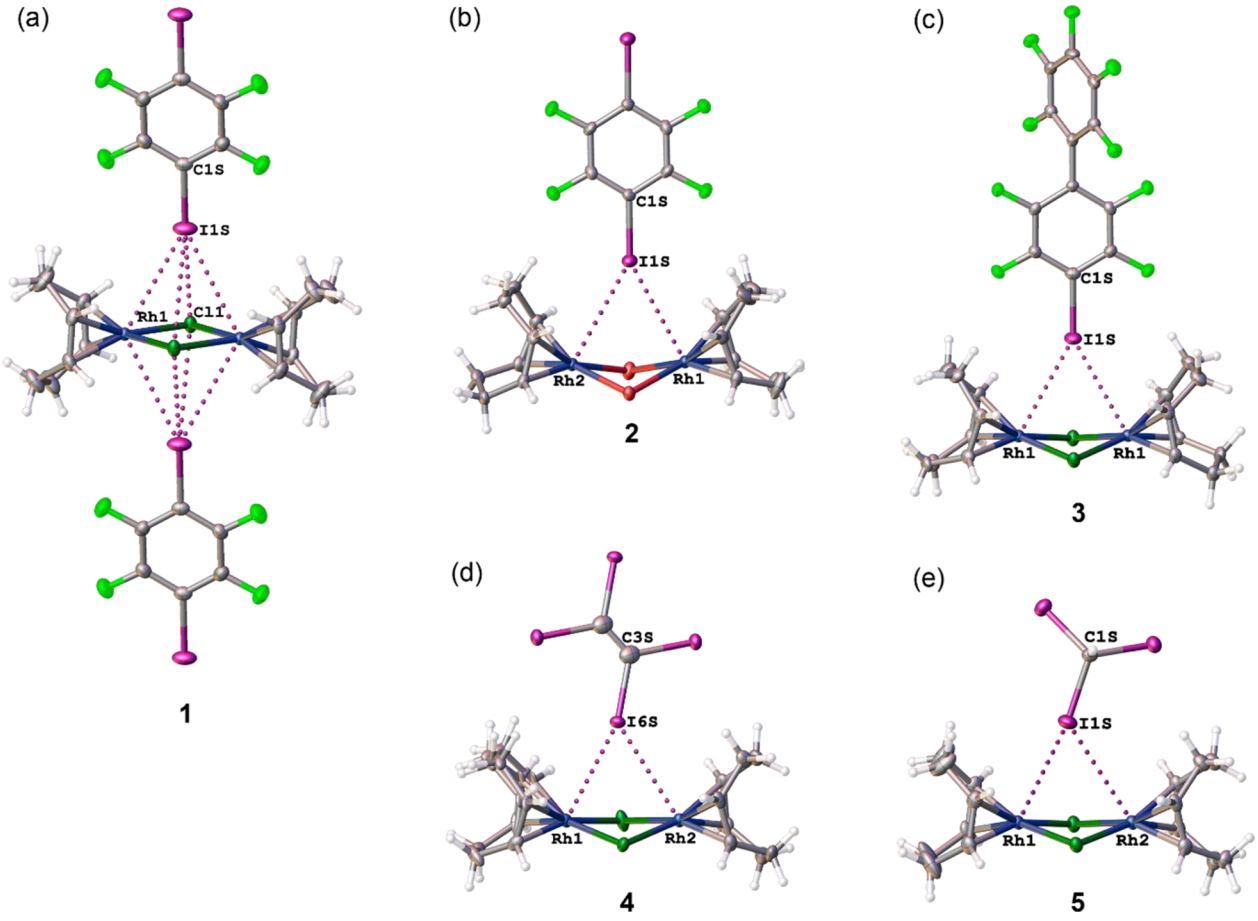

Figure 1. $Ar^F(\mu_4\text{-I})\cdots[Rh_2Cl_2]$ and $R^{EWG}(\mu_2\text{-I})\cdots[Rh,Rh]$ interactions in **1** (a), **2** (b), **3** (c), **4** (d), and **5** (e). Hereinafter the contacts shorter than ΣR_{vdW} are given by dotted lines, and thermal ellipsoids are shown with the 50% probability.

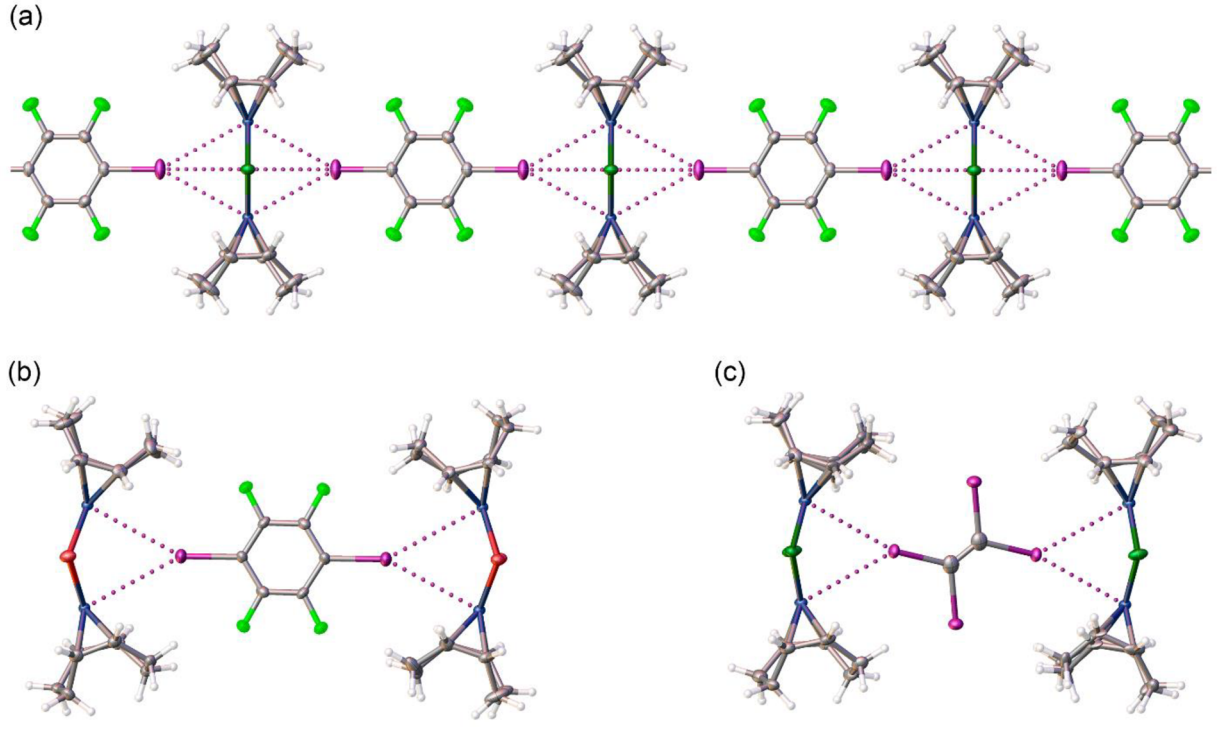

Figure 2. 1D-chain (a) and the isolated clusters (b,c) formed by the $Ar^F(\mu_4\text{-I})\cdots[Rh_2Cl_2]$ (**1**) and $R^{EWG}(\mu_2\text{-I})\cdots[Rh,Rh]$ (**2**, **4**) contacts.

https://dx.doi.org/10.1021/jacsau.1c00012
JACS Au 2021, 1, 354−361

Common to all structures is that I···Rh distances are significantly shorter than the sum of vdW radii (ΣR_{vdW}), considering the radius of I is 1.98 Å (the Bondi I radius[36]), and the radius of Rh is 2.02 Å (the Batsanov Rh radius;[37] the Rh radius is not given in the Bondi vdW radii list) (Table S3).

The most intriguing feature of the crystal structure of **1** is the unique *tetrafurcated* $Ar^F(\mu_4\text{-I})\cdots[Rh_2Cl_2]$ short contacts, where one I center of R^{EWG}–I interacts with all four atoms of the Rh_2Cl_2 core–thus forming 1D-chain $\cdots[Rh_2Cl_2]\cdots I(Ar^F)I\cdots[Rh_2Cl_2]\cdots$ involving XB between iodine atoms of the perfluoroarene linkers and the Rh_2Cl_2 cores (Figure 2a). Notably, such XB-involving assembly through simultaneously two metal centers had not been conducted before this study.

In contrast to **1**, the crystal structure of **2** featured two $[RhBr(COD)]_2$ per one $C_6F_4I_2$ entity; R^{EWG}–I links to the Rh_2Br_2 core of $[RhBr(COD)]_2$ via two bifurcated $R^{EWG}(\mu_2\text{-I})\cdots[Rh,Rh]$ short contacts (Figure 2b). This assembly results in a distortion of the Rh_2Br_2 entity, where the Rh atoms are tilted toward an I center of $C_6F_4I_2$. A similar 2:1 supramolecular cluster was found in **4** (Figure 2c). In the structures of **3** and **5**, R^{EWG}–I and $[RhCl(COD)]_2$ form 1:1 isolated clusters (Figure 1c,e), which are linked to each other via $R^{EWG}(\mu_2\text{-I})\cdots[Rh,Rh]$ interactions. One of these contacts, namely C1S–I1S···Rh1 in **5**, is the shortest one (3.4255(5) Å) among the other iodine–rhodium(I) contacts observed in this study. Other types of noncovalent interactions in the studied systems are represented by hydrogen bonds (HBs) and lone pair–π-hole (LP–π) interactions and are considered in Sections S1.3–1.4.

The variable-temperature XRD studies for **1** and **3** (five XRD experiments with heating from 100 to 300 K with 50 K per step), taken as examples, were performed to compare the response of the detected intermolecular contacts on temperature (Section S2). The $R^{EWG}(\mu_2\text{-I})\cdots[Rh,Rh]$ contacts in both structures were found to be pronouncedly less flexible with respect to the temperature change than the HBs and LP–π interactions. The largest lengthening of interatomic distances corresponding to the $R^{EWG}(\mu_2\text{-I})\cdots[Rh,Rh]$ interactions is observed for C1S–I1S···Rh1 contact in **3**; the I1S···Rh1 distance increases on 0.062 Å upon heating with 3.5952(6) Å at 100 K (Table S8).

Our search and processing of the Cambridge Structural Database (CSD) revealed only three relevant structures featuring $I\cdots[Rh^I]$ short contacts (Section S3), whose geometric features are substantially different for all three structures and are consistent with coordinative XB,[34] XB,[1] and semicoordination[38] bonding (Table S9). In structure NOCNOL (Figure S5b), we identified the previously overlooked C6–I1···Rh1 contact between two [Rh(acac)(CO){P(C_6F_4I-2)Ph_2}] entities, with geometric characteristics specific to $[d^8M]$-involving XB;[24,27,28] this contact exhibits interatomic distance (d(I1···Rh1) 3.5776(5) Å) less than ΣR_{vdW} (4.00 Å) and angle distribution around the I atom (∠(C6–I1···Rh1) 169.02(8)°) corresponding to XB according to the IUPAC criteria.[1]

We used the DFT study in combination to MEP, QTAIM, NCIplot, natural bond orbital (NBO), and ELF computational tools to shed light on the nature of the Rh^I-involving interactions. The molecular electrostatic potential (MEP) surfaces of the three XB donor molecules are represented in Figure S6. As expected, the iodoform presents the less intense σh (+25.7 kcal/mol, Figure S6a) and for $C_6F_4I_2$ and $C_{12}F_9I$ σhs (+33.2 and +35.0 kcal/mol, respectively) are larger and more intense. The MEP surfaces of the $[RhCl(COD)]_2$ complex in both conformations (planar and nonplanar Rh_2Cl_2 core) are given in Figure 3. In the planar conformation, the minimum

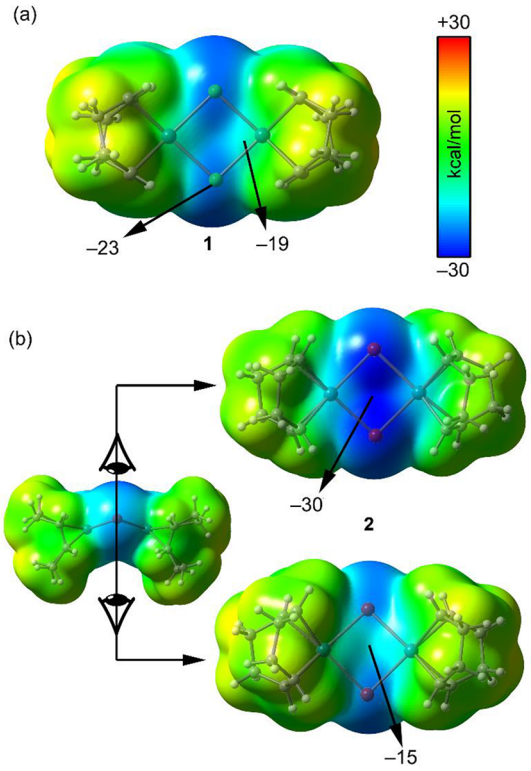

Figure 3. MEP surfaces (0.001 au) of the $[RhCl(COD)]_2$ complex in a planar (a) and nonplanar (b) conformations (two views) at the M06-2X/def2-TZVP level of theory. The values at selected points of the surfaces are given in kcal/mol.

value of MEP is located at the Cl atoms (−23 kcal/mol), and it is slightly reduced at the Rh atoms (−19 kcal/mol). In the nonplanar conformation, the minimum value is found between the Cl atoms (−30 kcal/mol), and the value at the opposite site is reduced to −15 kcal/mol. Therefore, the MEP analysis reveals that the $Ar^F(\mu_4\text{-I})\cdots[Rh_2Cl_2]$ and $R^{EWG}(\mu_2\text{-I})\cdots[Rh,Rh]$ interactions are electrostatically favorable, where the electron-rich Rh_2Cl_2 core interacts with the σh at the I atom, as is typical in XB.

The results of QTAIM analysis and DFT calculations are gathered in Figure 4 (for **1**–**2**) and Figure S7 (**3**–**5**). The distribution of bond critical points (CPs) and bond paths in the dimer of **1** reveals that the I atom is connected to the four atoms of the Rh_2Cl_2 core by means of four CPs. The value of ρ(r) at the bond CP3 (connecting the I to the closest Cl atom) is the largest one. In **2**–**5**, the I atom is interconnected to both Rh atoms of the core by two bond CPs and bond paths. Remarkably, in these complexes, it is not connected to the bridging Cl/Br ligands because of the different geometry of the Rh_2X_2 core compared with **1**. The values of ρ(r) at the bond CPs that characterize the I···Rh interaction correlate with the experimental distances (Table S3), that is, the ρ(r) values at the CPs increase as the I···Rh distance decrease. In Figures 4 and S7, we also included the interaction energies that are moderately strong, ranging from −8.05 kcal/mol to −9.89 kcal/mol, in agreement with the MEP analysis commented above (Figures 3 and S6). The QTAIM analysis reveals that there are additional interactions that also stabilize the assembly apart from the $R^{EWG}(\mu_2\text{-I})\cdots[Rh,Rh]$ interaction, which are C–H···F and/or C–H···I contacts. To measure the contribution of the $R^{EWG}(\mu_2\text{-I})\cdots[Rh,Rh]$ interaction, some theoretical models (Figures 4c,d and S7d–f) were

https://dx.doi.org/10.1021/jacsau.1c00012
JACS Au 2021, 1, 354–361

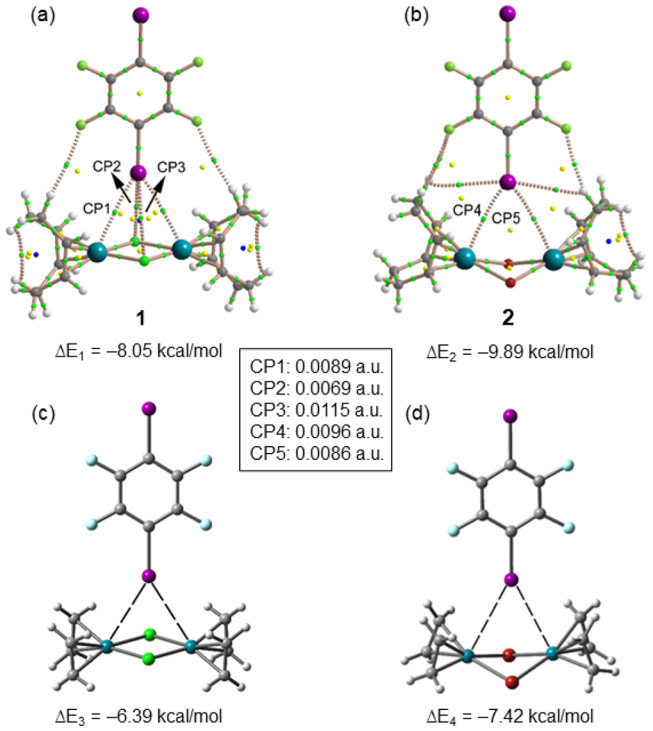

Figure 4. (a,b) AIM distribution of bond, ring, and cage critical points (green, yellow, and blue spheres, respectively) and bond paths for compounds **1** and **2**. (c,d) Theoretical models used to evaluate the $R^{EWG}(\mu_2\text{-I})\cdots[Rh,Rh]$ interactions.

used where the COD was simplified (replaced by two ethene units) and, consequently, the C–H···F/I are not formed. The interaction energies of the mutated complexes are given at the bottom of figures and reveal that the $R^{EWG}(\mu_2\text{-I})\cdots[Rh,Rh]$ interaction ranges from −6.4 to −7.56 kcal/mol, thus similar to strong H-bonding. By comparing the interaction energies of the whole systems to those of the mutated systems, it can be concluded that the $R^{EWG}(\mu_2\text{-I})\cdots[Rh,Rh]$ XB interaction clearly dominates the formation of the assemblies.

The noncovalent interaction plot (NCIplot) has been also computed because it is convenient to identify which regions in a supramolecular complex interact (Figures 5 and S8). In **1**–**5**, the shape and extension of the green (meaning weak attractive)

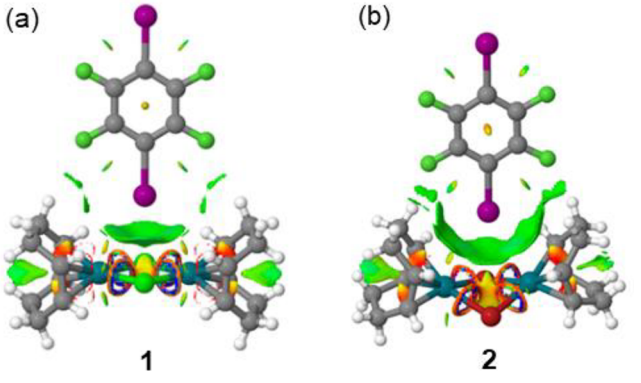

Figure 5. NCI surfaces of the dimers of **1** (a) and **2** (b). The gradient cutoff is ρ = 0.04, the isosurface is s = 0.35 au, and the color scale is $-0.04 < \text{sign}(\lambda_2)\rho < 0.04$ au. NCI surfaces for the dimers of **3**–**5** are given in Figure S8.

isosurfaces clearly demonstrate that indeed the interaction of the C–I bond is with the whole $[Rh_2Cl_2]$ core with some participation of the C–H bonds of the COD ligand. Therefore, the energetic MEP and NCIplot results indicate that the interaction between the XB donor molecules and the $[RhX(COD)]_2$ can be defined as an XB, where the whole Rh_2X_2 core interacts as an unconventional electron donor.

Further insight into the nature of the I···Rh interactions can be gained from the 3D electron deformation density (EDD) plot (Figure 6) as it provides information on charge concentration

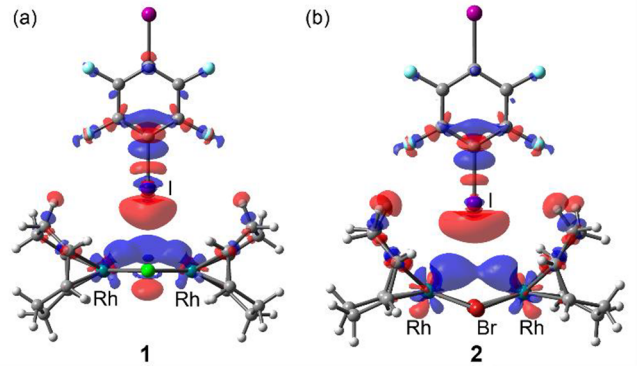

Figure 6. Theoretical (M06–2x/def2-TZVP) 3D electron deformation density (EDD) plots in **1** (a) and **2** (b). CC and CD values are represented by blue and red colors. $\Delta\rho(r)$ isosurfaces are drawn at 0.005 au.

(CC) and charge depletion (CD) regions in the molecule. In the case of **1**, the 3D EDD plot clearly depicts the charge depletion region of I facing an extended charge concentration region on both Rh-atoms and one Cl atom of the planar Rh_2Cl_2 core. In **2**, the 3D EDD plot is slightly different, showing that the CC region is located at the Rh-atoms, without any participation of the bromine atoms. Moreover, the CD region of I is significantly polarized toward both Rh atoms. This EDD analysis supports the halogen bonding nature of the $R^{EWG}(\mu_2\text{-I})\cdots[Rh,Rh]$ contacts and evidence that in both complexes the interaction is attractive in nature, in agreement with the NCIplot and energetic analyses. Finally, the EDD plots also reveal higher charge displacement for the H atoms of COD pointing to the perfluoroarene molecule in the adduct of compound **2** compared with **1**, in line with the QTAIM distribution of CPs and NCIplot shown in Figures 4–5.

In an effort to investigate the existence of LP → σ^*(C–I) interactions in compounds **1** and **2**, we have performed a NBO analysis focusing on the second-order perturbation analysis, since it is convenient to evaluate donor–acceptor interactions. The results are summarized in Table S10, where we gather all orbital donor–acceptor interactions involving the antibonding C–I bond and their concomitant stabilization energy, $E^{(2)}$. In both complexes, we found two contributions, one from the filled d_z^2(Rh) orbital to the empty σ^*(C–I) and a second contribution from one free LP of the halogen atom to the σ^*(C–I). In case of **1**, the latter contribution [LP(Cl) → σ^*(C–I)] is more relevant than the former d_z^2(Rh) → σ^*(C–I)]. In contrast, in compound **2**, the LP(Br) → σ^*(C–I) is negligible, and the most important contribution is the d_z^2(Rh) → σ^*(C–I), which is slightly larger than that of compound **1**, in line with the distortion of the Rh_2Br_2 core in **2**, where the Rh atoms are tilted toward an I center of $C_6F_4I_2$.

https://dx.doi.org/10.1021/jacsau.1c00012
JACS Au 2021, 1, 354–361

To further verify whether the observed I···Rh contacts are XBs, we performed Electron Localization Function (ELF) analysis for **1**−**5**. A combination of the ELF and QTAIM methods is represented in Figures 7 and S9; ELF projections for

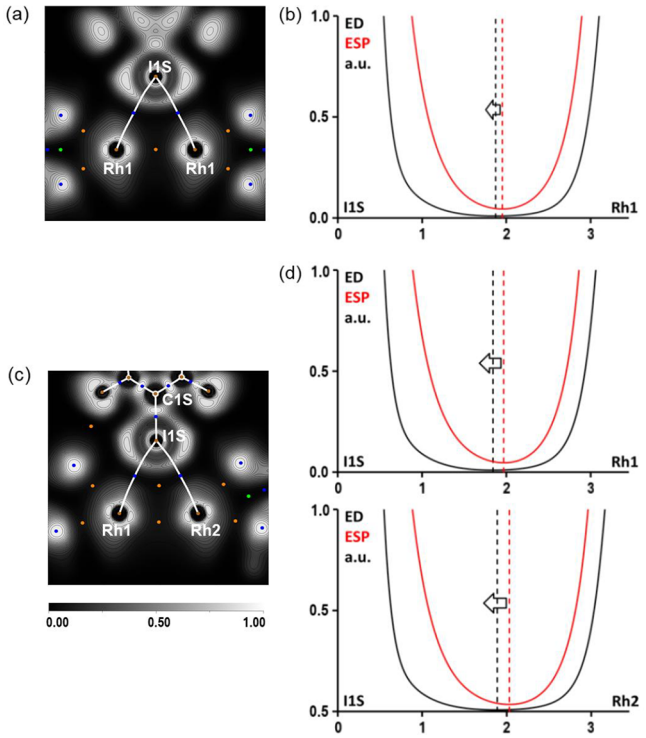

Figure 7. Left panel: the ELF projection and bond paths (white lines) for the $R^{EWG}(\mu_2\text{-I})\cdots[Rh,Rh]$ contacts in **1** (a) and **2** (c) (bond CPs (3, −1) are shown in blue, nuclear CPs (3, −3) − in pale brown, ring CPs (3, +1) − in orange, cage CPs (3, +3) − in green). Right panel: criterion $\rho(r)_{min}$ vs $\varphi(r)_{min}$: the ED (black) and the ESP (red) for the $R^{EWG}(\mu_2\text{-I})\cdots[Rh,Rh]$ interactions in **1** (b) and **2** (d) (interatomic distances are given in Å).

the $Ar^F(\mu_4\text{-I})\cdots[Rh_2Cl_2]$ and $R^{EWG}(\mu_2\text{-I})\cdots[Rh,Rh]$ contacts were plotted along with CPs and bond paths. The inspection of the ELF data proves the XB nature of the $Ar^F(\mu_4\text{-I})\cdots[Rh_2Cl_2]$ and $R^{EWG}(\mu_2\text{-I})\cdots[Rh,Rh]$ interactions, where Rh and Cl centers of $[RhX(COD)]_2$ function as nucleophiles, while the I centers of R^{EWG}Is are electrophiles.

To determine the philicity of interacting atoms, the analysis of the order of the electron density (ED; $\rho(r)_{min}$) and electrostatic potential (ESP; $\varphi(r)_{min}$) minima along bond paths were performed; this approach was previously applied for XB identification in crystals.[39−41] According to this method, $\varphi(r)_{min}$ is shifted toward the nucleophilic atom, while $\rho(r)_{min}$ is shifted toward the electrophilic atom.

The 1D profiles of the ED and ESP functions along the I···Rh bond paths confirmed the nucleophilic nature of Rh atoms toward I centers of R^{EWG}Is (Figure 7 (right panel) and Figure S10). Indeed, the significant shifts of the ESP minima to the Rh electron density basins were observed in all cases apart from the two I···Rh contacts in **4** and **5** (Section S4.6). In **1**, the 1D profiles of the ED and ESP functions along the I1S···Cl1 BPs (Figure S10a) provide evidence that the ESP minima belong to the Cl electron density basins, which means that partially Cl electrons are drifted to the I center. Hence, one can state that the iodine···metal interactions can be formulated as the $Ar^F(\mu_4\text{-I})\cdots[Rh_2Cl_2]$ (for **1**) and $R^{EWG}(\mu_2\text{-I})\cdots[Rh,Rh]$ (for **2** and **3**) XBs, while two I···Rh contacts in **4** and **5** are the conventional two-center $R^{EWG}I\cdots[Rh^I]$ XBs.

CONCLUSIONS

We examined the geometric and energetic features of the I···$[Rh^I]$ interactions using the combined experimental and theoretical approaches to arrive at a comprehensive understanding of these forces involved where positively charged rhodium(I) centers are functioning as Lewis bases. We demonstrated that the $[RhX(COD)]_2$ (X = Cl, Br) complexes can be cocrystallized with R^{EWG}−Is forming cocrystals **1**−**5**. Upon analysis of noncovalent forces in the XRD structures of **1**−**5**, in addition to rather conventional intermolecular contacts, we recognized hitherto unknown $Ar^F(\mu_4\text{-I})\cdots[Rh_2Cl_2]$ and $R^{EWG}(\mu_2I)\cdots[Rh,Rh]$ interactions involving iodine centers of σh donors and $[Rh_2X_2]$ metal cores of the rhodium(I) complexes. The noncovalent XB nature of the detected contacts was confirmed theoretically by the DFT calculations using several computational tools (QTAIM, DFT energies, NCI and EDD plots, MEP surfaces, ELF analysis).

To summarize, we found the three-center XB that involves simultaneously two metal centers functioning as integrated σh acceptor toward iodine(I)-based σh donors. Moreover, we performed the assembly through two- or more metal-involving XBs exploring the potential of $\cdots[Rh_2Cl_2]\cdots I(Ar^F)I\cdots[Rh_2Cl_2]\cdots$ or tetrafurcated $Ar^F(\mu_4\text{-I})\cdots[Rh_2Cl_2]$ interactions.

EXPERIMENTAL SECTION

Starting Materials and Cocrystallization

$RhCl_3\cdot3H_2O$, $RhBr_3\cdot3H_2O$, 1,5-cyclooctadiene, Na_2CO_3, 1,4-$C_6F_4I_2$, C_2I_4, CHI_3, and all solvents were obtained from commercial sources and used as received; $C_{12}F_9I$[42] and $[RhX(COD)]_2$ (X = Cl, Br)[43] were synthesized via previously published procedures.

Single crystals of **1**−**3** and **5** were obtained by slow evaporation of a dichloromethane solution (4 mL) of a mixture of the corresponding $[RhX(COD)]_2$ (14 mmol) and R^{EWG}−I taken in 1:1 molar ratio at RT. Single crystals of **4** were prepared from a dichloromethane−nitromethane solution (1:1, v/v, 4 mL) of a mixture of $[RhCl(COD)]_2$ (7 mg, 14 mmol) and C_2I_4 (7 mg, 14 mmol); the reaction mixture was stirred under ultrasonic treatment for complete homogenization, and then left to stand at RT for slow evaporation. Yellow crystals of **1**−**5** suitable for XRD were released after 3−4 d.

X-ray Structure Determinations

Suitable single crystals of **1**−**5** were studied on a Bruker Apex II Duo CCD diffractometer (Mo Kα (λ = 0.71073), graphite monochromator, ω-scans). The crystals of **2**, **4**, and **5** were kept at 120 K during data collection. The intensity data were integrated by the SAINT program[44] and were corrected for absorption and decay using SADABS.[45] All structures were solved by direct methods using SHELXS[44] and refined against F^2 using SHELXL-2018.[46] All non-hydrogen atoms were refined with individual anisotropic displacement parameters. The hydrogen atoms in all structures were placed in ideal calculated positions and refined as riding atoms with relative isotropic displacement parameters.

Variable-temperature single-crystal XRD studies of **1** and **3** were performed using Bruker APEX II DUO diffractometer equipped with Oxford Cryosystems Cobra low-temperature device and CCD detector. Diffraction data sets were collected (Mo Kα radiation, graphite monochromator, ω-scans) at five temperatures (100, 150, 200, 250, 300 K) for the same crystal sample once mounted on a glass needle using two-part adhesive. No structural phase transitions have been detected for crystals **1** and **3** in the studied temperature range.

The main crystallography data and refinement details are listed in Tables S1, S6−S7. CCDC numbers 2054735−2054747 contain all supporting structural and refinement data.

https://dx.doi.org/10.1021/jacsau.1c00012
JACS Au 2021, 1, 354−361

Computational Details

The energetic features of the complexes included in this study were calculated at the M06-2X/def2-TZVP[29] level of theory using the crystallographic coordinates. For the calculations, the GAUSSIAN-16 program has been used.[47] The basis set superposition error for the calculation of interaction energies has been corrected using the counterpoise method.[48] The MEP surfaces have been computed at the same level of theory and represented using the 0.001 au isosurface. The NCI plot index[49] computational tool has been used to characterize noncovalent interactions using the M06-2X/def2-TZVP level wave function. They correspond to both favorable and unfavorable interactions, as differentiated by the sign of the second density Hessian eigenvalue and defined by the isosurface color. The color scheme is a red-yellow-green-blue scale with red for ρ^{+}_{cut} (repulsive) and blue for ρ^{-}_{cut} (attractive). Yellow and green isosurfaces correspond to weakly repulsive and attractive interactions, respectively. The QTAIM analysis[50] has been performed using the AIMAll program at the same level of theory.[51] The EDD plots were computed using the M06-2X/def2-TZVP wave function by means of the MULTIWFN v. 3.7 program[52] by considering the halogen donor and metal complex as fragments. The EDD grid data generated with the MULTIWFN v. 3.7 program was saved as a cube file and visualized using Gaussview program.[53] The NBO 3.1 has been used to evaluate donor−acceptor interactions[54] as implemented in GAUSSIAN-16. The ELF analysis[55−58] has been performed in MULTIWFN 3.7.[52]

■ ASSOCIATED CONTENT

Supporting Information

The Supporting Information is available free of charge at https://pubs.acs.org/doi/10.1021/jacsau.1c00012.

XRD studies (Sections S1−S2), processing of the CSD (Section S3), and theoretical calculations (Section S4) (PDF)

Accession Codes

Supporting crystallographic data have been deposited at Cambridge Crystallographic Data Centre (CCDC 2054735−2054747) and can be obtained free of charge via www.ccdc.cam.ac.uk/data_request/cif.

■ AUTHOR INFORMATION

Corresponding Authors

Antonio Frontera − *Department of Chemistry, Universitat de les Illes Balears, 07122 Palma de Mallorca (Baleares), Spain;* orcid.org/0000-0001-7840-2139; Email: toni.frontera@uib.es

Vadim Yu. Kukushkin − *Institute of Chemistry, Saint Petersburg State University, 199034 Saint Petersburg, Russian Federation; Laboratory of Crystal Engineering of Functional Materials, South Ural State University, 454080 Chelyabinsk, Russian Federation;* orcid.org/0000-0002-2253-085X; Email: v.kukushkin@spbu.ru

Authors

Anastasiya A. Eliseeva − *Institute of Chemistry, Saint Petersburg State University, 199034 Saint Petersburg, Russian Federation;* orcid.org/0000-0003-2982-3804

Daniil M. Ivanov − *Institute of Chemistry, Saint Petersburg State University, 199034 Saint Petersburg, Russian Federation;* orcid.org/0000-0002-0855-2251

Anton V. Rozhkov − *Institute of Chemistry, Saint Petersburg State University, 199034 Saint Petersburg, Russian Federation;* orcid.org/0000-0002-8658-7281

Ivan V. Ananyev − *A. N. Nesmeyanov Institute of Organoelement Compounds, Russian Academy of Sciences, 119991 Moscow, Russian Federation;* orcid.org/0000-0001-6867-7534

Complete contact information is available at: https://pubs.acs.org/10.1021/jacsau.1c00012

Author Contributions

A.A.E.−conceptualization, investigation, writing; D.M.I.−conceptualization; A.V.R.−investigation; I.V.A.−investigation; A.F.−computational study, writing; V.Y.K.−conceptualization, writing, project administration.

Notes

The authors declare no competing financial interest.

■ ACKNOWLEDGMENTS

This study represents an integration of two diverse funded projects: a part on crystal engineering was supported by the Russian Science Foundation (Project 20-13-00144), while the synthetic and physicochemical studies were funded by the Council for Grants of the President of Russian Federation (Project MK-1614.2021.1.3). I.V.A. thanks the Ministry of Science and Higher Education for supporting XRD facilities. The support of MICIU/AEI, CTQ2017-85821-R, Feder funds (computation studies by A.F.) are gratefully acknowledged.

■ ABBREVIATIONS

XB, halogen bond(ing); σh, σ-hole; COD, 1,5-cyclooctadiene; R^{EWG}−I, organic iodine(I)-based species featuring electron-withdrawing group; XRD, X-ray diffraction; ΣR_{vdW}, sum of vdW radii; HB, hydrogen bond; LP−π, lone pair−π-hole interaction; CSD, Cambridge Structural Database; MEP, molecular electrostatic potential; CP, bond critical point; NCIplot, noncovalent interaction plot; EDD, electron deformation density; CC, charge concentration; CD, charge depletion; NBO, natural bond orbital; ELF, electron localization function; ED, electron density; ESP, electrostatic potential; CCDC, Cambridge Crystallographic Data Centre.

■ REFERENCES

(1) Desiraju, G. R.; Ho, P. S.; Kloo, L.; Legon, A. C.; Marquardt, R.; Metrangolo, P.; Politzer, P.; Resnati, G.; Rissanen, K. Definition of the Halogen Bond (IUPAC Recommendations 2013). *Pure Appl. Chem.* **2013**, *85* (8), 1711−1713.

(2) Cavallo, G.; Metrangolo, P.; Milani, R.; Pilati, T.; Priimagi, A.; Resnati, G.; Terraneo, G. The Halogen Bond. *Chem. Rev.* **2016**, *116* (4), 2478−2601.

(3) *Non-Covalent Interactions in the Synthesis and Design of New Compounds*; Maharramov, A. M., Mahmudov, K. T., Kopylovich, M. N., Pombeiro, A. J. L., Eds.; John Wiley & Sons Inc.: Hoboken, NJ, 2016.

(4) Brammer, L. Halogen Bonding, Chalcogen Bonding, Pnictogen Bonding, Tetrel Bonding: Origins, Current Status and Discussion. *Faraday Discuss.* **2017**, *203*, 485−507.

(5) Politzer, P.; Murray, J. An Overview of Strengths and Directionalities of Noncovalent Interactions: σ-Holes and π-Holes. *Crystals* **2019**, *9* (3), 165.

(6) Fave, C.; Schöllhorn, B. Electrochemical Activation of Halogen Bonding. *Curr. Opin. Electrochem.* **2019**, *15*, 89−96.

(7) Alkorta, I.; Elguero, J.; Frontera, A. Not Only Hydrogen Bonds: Other Noncovalent Interactions. *Crystals* **2020**, *10* (3), 180.

(8) Gilday, L. C.; Robinson, S. W.; Barendt, T. A.; Langton, M. J.; Mullaney, B. R.; Beer, P. D. Halogen Bonding in Supramolecular Chemistry. *Chem. Rev.* **2015**, *115* (15), 7118−7195.

(9) Mukherjee, A.; Sanz-Matias, A.; Velpula, G.; Waghray, D.; Ivasenko, O.; Bilbao, N.; Harvey, J. N.; Mali, K. S.; De Feyter, S. Halogenated Building Blocks for 2D Crystal Engineering on Solid Surfaces: Lessons from Hydrogen Bonding. *Chem. Sci.* **2019**, *10* (13), 3881−3891.
(10) Wang, H.; Bisoyi, H. K.; Urbas, A. M.; Bunning, T. J.; Li, Q. The Halogen Bond: An Emerging Supramolecular Tool in the Design of Functional Mesomorphic Materials. *Chem. - Eur. J.* **2019**, *25* (6), 1369−1378.
(11) Mahmudov, K. T.; Kopylovich, M. N.; Guedes da Silva, M. F. C.; Pombeiro, A. J. L. Non-Covalent Interactions in the Synthesis of Coordination Compounds: Recent Advances. *Coord. Chem. Rev.* **2017**, *345*, 54−72.
(12) Berger, G.; Soubhye, J.; Meyer, F. Halogen Bonding in Polymer Science: From Crystal Engineering to Functional Supramolecular Polymers and Materials. *Polym. Chem.* **2015**, *6* (19), 3559−3580.
(13) Mahmudov, K. T.; Gurbanov, A. V.; Guseinov, F. I.; Guedes da Silva, M. F. C. Noncovalent Interactions in Metal Complex Catalysis. *Coord. Chem. Rev.* **2019**, *387*, 32−46.
(14) Bulfield, D.; Huber, S. M. Halogen Bonding in Organic Synthesis and Organocatalysis. *Chem. - Eur. J.* **2016**, *22* (41), 14434−14450.
(15) Benz, S.; Poblador-Bahamonde, A. I.; Low-Ders, N.; Matile, S. Catalysis with Pnictogen, Chalcogen, and Halogen Bonds. *Angew. Chem., Int. Ed.* **2018**, *57* (19), 5408−5412.
(16) Tepper, R.; Schubert, U. S. Halogen Bonding in Solution: Anion Recognition, Templated Self-Assembly, and Organocatalysis. *Angew. Chem., Int. Ed.* **2018**, *57* (21), 6004−6016.
(17) Ho, P. S. Halogen Bonding in Medicinal Chemistry: From Observation to Prediction. *Future Med. Chem.* **2017**, *9* (7), 637−640.
(18) Dalpiaz, A.; Pavan, B.; Ferretti, V. Can Pharmaceutical Co-Crystals Provide an Opportunity to Modify the Biological Properties of Drugs? *Drug Discovery Today* **2017**, *22* (8), 1134−1138.
(19) Bayse, C. A. Halogen Bonding from the Bonding Perspective with Considerations for Mechanisms of Thyroid Hormone Activation and Inhibition. *New J. Chem.* **2018**, *42* (13), 10623−10632.
(20) Bikbaeva, Z. M.; Ivanov, D. M.; Novikov, A. S.; Ananyev, I. V.; Bokach, N. A.; Kukushkin, V. Y. Electrophilic−Nucleophilic Dualism of Nickel(II) toward Ni···I Noncovalent Interactions: Semicoordination of Iodine Centers via Electron Belt and Halogen Bonding via σ-Hole. *Inorg. Chem.* **2017**, *56* (21), 13562−13578.
(21) Kucheriv, O. I.; Shylin, S. I.; Ksenofontov, V.; Dechert, S.; Haukka, M.; Fritsky, I. O.; Gural'skiy, I. A. Spin Crossover in Fe(II)−M(II) Cyanoheterobimetallic Frameworks (M = Ni, Pd, Pt) with 2-Substituted Pyrazines. *Inorg. Chem.* **2016**, *55* (10), 4906−4914.
(22) Yamashina, Y.; Kataoka, Y.; Ura, Y. Inclusion of an Iodine Molecule in a Tiara-Like Octanuclear Palladium Thiolate Complex. *Eur. J. Inorg. Chem.* **2014**, *2014* (25), 4073−4078.
(23) Baykov, S. V.; Dabranskaya, U.; Ivanov, D. M.; Novikov, A. S.; Boyarskiy, V. P. Pt/Pd and I/Br Isostructural Exchange Provides Formation of C−I···Pd, C−Br···Pt, and C−Br···Pd Metal-Involving Halogen Bonding. *Cryst. Growth Des.* **2018**, *18* (10), 5973−5980.
(24) Gossage, R. A.; Ryabov, A. D.; Spek, A. L.; Stufkens, D. J.; van Beek, J. A. M.; van Eldik, R.; van Koten, G. Models for the Initial Stages of Oxidative Addition. Synthesis, Characterization, and Mechanistic Investigation of η^1-I_2 Organometallic "Pincer" Complexes of Platinum. X-ray Crystal Structures of $[PtI(C_6H_3\{CH_2NMe_2\}_2\text{-}2,6)(\eta^1\text{-}I_2)]$ and *exo-meso*-$[Pt(\eta^1\text{-}I_3)(\eta^1\text{-}I_2)(C_6H_3\{CH_2N(t\text{-}Bu)Me\}_2\text{-}2,6)]$. *J. Am. Chem. Soc.* **1999**, *121* (11), 2488−2497.
(25) Ivanov, D. M.; Novikov, A. S.; Ananyev, I. V.; Kirina, Y. V.; Kukushkin, V. Y. Halogen Bonding between Metal Centers and Halocarbons. *Chem. Commun.* **2016**, *52* (32), 5565−5568.
(26) Dabranskaya, U.; Ivanov, D. M.; Novikov, A. S.; Matveychuk, Y. V.; Bokach, N. A.; Kukushkin, V. Y. Metal-Involving Bifurcated Halogen Bonding C−Br···η^2(Cl−Pt). *Cryst. Growth Des.* **2019**, *19* (2), 1364−1376.
(27) Rozhkov, A. V.; Ivanov, D. M.; Novikov, A. S.; Ananyev, I. V.; Bokach, N. A.; Kukushkin, V. Y. Metal-Involving Halogen Bond Ar−I···$[d_z^2Pt^{II}]$ in a Platinum Acetylacetonate Complex. *CrystEngComm* **2020**, *22* (3), 554−563.
(28) Katlenok, E. A.; Haukka, M.; Levin, O. V.; Frontera, A.; Kukushkin, V. Y. Supramolecular Assembly of Metal Complexes by (Aryl)I···$d_z^2[Pt^{II}]$ Halogen Bond. *Chem. - Eur. J.* **2020**, *26* (34), 7692−7701.
(29) Komoto, Y.; Fujii, S.; Hara, K.; Kiguchi, M. Single Molecular Bridging of Au Nanogap Using Aryl Halide Molecules. *J. Phys. Chem. C* **2013**, *117* (46), 24277−24282.
(30) Blakey, I.; Merican, Z.; Rintoul, L.; Chuang, Y.-M.; Jack, K. S.; Micallef, A. S. Interactions of Iodoperfluorobenzene Compounds with Gold Nanoparticles. *Phys. Chem. Chem. Phys.* **2012**, *14* (10), 3604−3611.
(31) Yamamoto, H. M.; Yamaura, J.-I.; Kato, R. Multicomponent Molecular Conductors with Supramolecular Assembly: Iodine-Containing Neutral Molecules as Building Blocks. *J. Am. Chem. Soc.* **1998**, *120* (24), 5905−5913.
(32) Shaffer, D. W.; Ryken, S. A.; Zarkesh, R. A.; Heyduk, A. F. Ligand Effects on the Oxidative Addition of Halogens to (dpp-nacnac^R)Rh-(phdi). *Inorg. Chem.* **2012**, *51* (22), 12122−12131.
(33) Rogachev, A. Y.; Hoffmann, R. Iodine (I_2) as a Janus-Faced Ligand in Organometallics. *J. Am. Chem. Soc.* **2013**, *135* (8), 3262−3275.
(34) Rissanen, K.; Haukka, M. Halonium Ions as Halogen Bond Donors in the Solid State $[XL_2]Y$ Complexes. In *Topics in Current Chemistry. Halogen Bonding II*; Metrangolo, P., Resnati, G., Eds.; Springer International Publishing: Cham, Switzerland, 2015; Vol. *359*, pp 77−90.
(35) Aakeröy, C. B.; Sinha, A. S. Co-crystals: Introduction and Scope. In *Co-Crystals: Preparation, Characterization and Applications*; Aakeröy, C. B., Sinha, A. S., Eds.; Monographs in Supramolecular Chemistry; Royal Society of Chemistry: Cambridge, 2018.
(36) Bondi, A. Van Der Waals Volumes and Radii. *J. Phys. Chem.* **1964**, *68* (3), 441−451.
(37) Batsanov, S. S. Van Der Waals Radii of Elements. *Inorg. Mater.* **2001**, *37* (9), 871−885.
(38) Valach, F. A Bond-Valence Approach to the Semicoordination of Copper-Oxygen and Copper−Nitrogen Complexes. *Polyhedron* **1999**, *18* (5), 699−706.
(39) Bartashevich, E. V.; Matveychuk, Y. V.; Troitskaya, E. A.; Tsirelson, V. G. Characterizing the Multiple Non-Covalent Interactions in N, S-Heterocycles−Diiodine Complexes with Focus on Halogen Bonding. *Comput. Theor. Chem.* **2014**, *1037*, 53−62.
(40) Bartashevich, E.; Yushina, I.; Kropotina, K.; Muhitdinova, S.; Tsirelson, V. Testing the Tools for Revealing and Characterizing the Iodine−iodine Halogen Bond in Crystals. *Acta Crystallogr., Sect. B: Struct. Sci., Cryst. Eng. Mater.* **2017**, *73* (2), 217−226.
(41) Bartashevich, E.; Mukhitdinova, S.; Yushina, I.; Tsirelson, V. Electronic Criterion for Categorizing the Chalcogen and Halogen Bonds: Sulfur−iodine Interactions in Crystals. *Acta Crystallogr., Sect. B: Struct. Sci., Cryst. Eng. Mater.* **2019**, *75* (2), 117−126.
(42) Rozhkov, A. V.; Eliseeva, A. A.; Baykov, S. V.; Galmés, B.; Frontera, A.; Kukushkin, V. Y. One-pot Route to X-Perfluoroarenes (X = Br, I) Based on Fe^{III}-Assisted C−F Functionalization and Utilization of These Arenes as Building Blocks for Crystal Engineering Involving Halogen Bonding. *Cryst. Growth Des.* **2020**, *20* (9), 5908−5921.
(43) Giordano, G.; Crabtree, R. H.; Heintz, R. M.; Forster, D.; Morris, D. E. Di-μ-Chloro-Bis(η^4-1,5-Cyclooctadiene)-Dirhodium(I). In *Inorganic Syntheses: Reagents for Transition Metal Complex and Organometallic Syntheses*; Angelici, R. J., Ed.; John Wiley & Sons, Inc.: New York, 1990; Vol. *28*, pp 1−8.
(44) Sheldrick, G. M. SHELXT − Integrated Space-Group and Crystal-Structure Determination. *Acta Crystallogr., Sect. A: Found. Adv.* **2015**, *71* (1), 3−8.
(45) Krause, L.; Herbst-Irmer, R.; Sheldrick, G. M.; Stalke, D. Comparison of Silver and Molybdenum Microfocus X-Ray Sources for Single-Crystal Structure Determination. *J. Appl. Crystallogr.* **2015**, *48* (1), 3−10.
(46) Sheldrick, G. M. Crystal Structure Refinement with SHELXL. *Acta Crystallogr., Sect. C: Struct. Chem.* **2015**, *71* (1), 3−8.

https://dx.doi.org/10.1021/jacsau.1c00012
JACS Au 2021, 1, 354−361

(47) Frisch, M. J.; Trucks, G. W.; Schlegel, H. B.; Scuseria, G. E.; Robb, M. A.; Cheeseman, J. R.; Scalmani, G.; Barone, V.; Petersson, G. A.; Nakatsuji, H.; Li, X.; Caricato, M.; Marenich, A. V.; Bloino, J.; Janesko, B. G.; Gomperts, R.; Mennucci, B.; Hratchian, H. P.; Ortiz, J. V.; Izmaylov, A. F.; Sonnenberg, J. L.; Williams-Young, D.; Ding, F.; Lipparini, F.; Egidi, F.; Goings, J.; Peng, B.; Petrone, A.; Henderson, T.; Ranasinghe, D.; Zakrzewski, V. G.; Gao, J.; Rega, N.; Zheng, G.; Liang, W.; Hada, M.; Ehara, M.; Toyota, K.; Fukuda, R.; Hasegawa, J.; Ishida, M.; Nakajima, T.; Honda, Y.; Kitao, O.; Nakai, H.; Vreven, T.; Throssell, K.; Montgomery, J. A. J.; Peralta, J. E.; Ogliaro, F.; Bearpark, M. J.; Heyd, J. J.; Brothers, E. N.; Kudin, K. N.; Staroverov, V. N.; Keith, T. A.; Kobayashi, R.; Normand, J.; Raghavachari, K.; Rendell, A. P.; Burant, J. C.; Iyengar, S. S.; Tomasi, J.; Cossi, M.; Millam, J. M.; Klene, M.; Adamo, C.; Cammi, R.; Ochterski, J. W.; Martin, R. L.; Morokuma, K.; Farkas, O.; Foresman, J. B.; Fox, D. J. *Gaussian 16*, Revision A.03; Gaussian, Inc.: Wallingford, CT, 2016.
(48) Boys, S. F.; Bernardi, F. The Calculation of Small Molecular Interactions by the Differences of Separate Total Energies. Some Procedures with Reduced Errors. *Mol. Phys.* **1970**, *19* (4), 553−566.
(49) Contreras-García, J.; Johnson, E. R.; Keinan, S.; Chaudret, R.; Piquemal, J.-P.; Beratan, D. N.; Yang, W. NCIPLOT: A Program for Plotting Noncovalent Interaction Regions. *J. Chem. Theory Comput.* **2011**, *7* (3), 625−632.
(50) Bader, R. F. W. A Quantum Theory of Molecular Structure and Its Applications. *Chem. Rev.* **1991**, *91* (5), 893−928.
(51) Keith, T. A. *AIMAll*; TK Gristmill Software: Overland Park, KS, 2019.
(52) Lu, T.; Chen, F. Multiwfn: A Multifunctional Wavefunction Analyzer. *J. Comput. Chem.* **2012**, *33* (5), 580−592.
(53) Dennington, R.; Keith, T. A.; Millam, J. M. *GaussView*; Semichem Inc.: Shawnee Mission, KS, 2016.
(54) Reed, A. E.; Curtiss, L. A.; Weinhold, F. Intermolecular Interactions from a Natural Bond Orbital, Donor-Acceptor Viewpoint. *Chem. Rev.* **1988**, *88* (6), 899−926.
(55) Becke, A. D.; Edgecombe, K. E. A Simple Measure of Electron Localization in Atomic and Molecular Systems. *J. Chem. Phys.* **1990**, *92* (9), 5397−5403.
(56) Silvi, B.; Savin, A. Classification of Chemical Bonds Based on Topological Analysis of Electron Localization Functions. *Nature* **1994**, *371* (6499), 683−686.
(57) Savin, A.; Nesper, R.; Wengert, S.; Fässler, T. F. ELF: The Electron Localization Function. *Angew. Chem., Int. Ed. Engl.* **1997**, *36* (17), 1808−1832.
(58) Fuentealba, P.; Chamorro, E.; Santos, J. C. Understanding and Using the Electron Localization Function. In *Theoretical Aspects of Chemical Reactivity*; Toro-Labbé, A., Ed.; Elsevier B.V.: Amsterdam, 2007; Vol. *19*, pp 57−85.

https://dx.doi.org/10.1021/jacsau.1c00012
JACS Au 2021, 1, 354−361